

Lawrence Berkeley National Laboratory

LBL Publications

Title

Nanoscale Copper and Copper Compounds for Advanced Device Applications

Permalink

<https://escholarship.org/uc/item/28m9p7g2>

Journal

Metallurgical and Materials Transactions A, 47(12)

ISSN

1073-5623

Author

Chen, Lih-Juann

Publication Date

2016-12-01

DOI

10.1007/s11661-016-3477-8

Peer reviewed

Nanoscale Copper and Copper Compounds for Advanced Device Applications

- [Authors](#)
- [Authors and affiliations](#)

• Lih-Juann Chen

• 

1. 1. Symposium: Micromechanics of Advanced Materials III in Honor of J.C.M. Li
First Online: 21 April 2016

• [284](#) Downloads

• [1](#) Citations

Abstract

Copper has been in use for at least 10,000 years. Copper alloys, such as bronze and brass, have played important roles in advancing civilization in human history. Bronze artifacts date at least 6500 years. On the other hand, discovery of intriguing properties and new applications in contemporary technology for copper and its compounds, particularly on nanoscale, have continued. In this paper, examples for the applications of Cu and Cu alloys for advanced device applications will be given on Cu metallization in microelectronics devices, Cu nanobats as field emitters, Cu₂S nanowire array as high-rate capability and high-capacity cathodes for lithium-ion batteries, Cu-Te nanostructures for field-effect transistor, Cu₃Si nanowires as high-performance field emitters and efficient anti-reflective layers, single-crystal Cu(In,Ga)Se₂ nanotip arrays for high-efficiency solar cell, multilevel Cu₂S resistive memory, superlattice Cu₂S-Ag₂S heterojunction diodes, and facet-dependent Cu₂O diode.

Keywords

Cu₂O Resistive Switching Nanowire Array Resistive Random Access Memory Bronze Artifact

These keywords were added by machine and not by the authors. This process is experimental and the keywords may be updated as the learning algorithm improves.

Manuscript submitted November 29, 2015.

1 Overview

Copper has been in use for at least 10,000 years and was the first metal to be used in large quantity. Copper alloys, such as bronze and brass, have played important roles in advancing civilization in human history. Bronze artifacts date at least 6500 years. Early uses of bronze included tools, weapons, armor, and building materials since they are harder and more durable than their stone and copper predecessors. Brass is used for decoration for its bright gold-like appearance; for applications where low friction is required such as locks, gears, bearings, doorknobs, ammunition casings, and valves; for plumbing, electrical applications, and zippers. It has also been used extensively in brass musical instruments such as horns and bells where a combination of high workability and durability is desired. Brass is often used in situations where it is important that sparks should not be struck, as in fittings and tools around explosive gases. The ability to resist corrosion ensured that copper, bronze, and brass remained as both functional and decorative materials during the Middle Ages and the successive centuries through the Industrial Revolution and on to the present day.[1,2] The electrification of the world in late nineteenth century had resulted in the widespread use of Cu wires both for transmission of electricity and for coils in electrical motors. In fact, Cu is still mostly used as electrical wires (~60 pct) nowadays.

The valuable properties of copper which were evident at the dawn of civilization were an attractive color, excellent ductility and malleability, and a capability of being hardened by working. In modern times, further properties have been appreciated and exploited across a wide range of applications: high thermal and electrical conductivities, excellent corrosion and biofouling resistance, and antimicrobial properties. Historically, the Age of Cu Alloys gave way to the Age of Iron, not because of the lack of strength, but chiefly because of the economic factor. Owing to the present high price of the metal, Cu and its alloys are being replaced by cheaper materials, such as Al and plastics, in many applications.[1,2] It is of interest that in a compilation of end-use applications for Cu and Cu alloys in the United States, high electrical conductivity is the major reason for choosing copper and Cu alloys in 9 of 16 categories, corrosion resistance a major reason in 8, ease of fabrication in 6, and good heat-transfer properties in 5.[3]

It is remarkable that in the Twenty-first century, Cu continues to find new ways into many main branches of technology. For example, Cu metallization in nanoelectronics devices, Cu oxide-based superconductors, Cu-In-Ga-Se (CIGS) solar materials, etc. Furthermore, discovery of intriguing properties and new applications in contemporary technology for copper and its compounds have continued. In this paper, we present several examples of nanoscale Cu and Cu compounds for advanced device applications.

2 Cu Metallization

2.1 Interfacial Reactions

Cu has gradually replaced Al as the interconnect material for IC devices since the turn of the century owing to its low resistivity and high electromigration resistance. In the nanoelectronics era, Cu interconnects have become ubiquitous.

Interfacial reactions of ultrahigh-vacuum-deposited Cu thin films on atomically cleaned (111)Si have been investigated. An interface compound, CuSi_x with $x = 11.2$ to 14 at. pct (ζ phase), was observed to be present at the Cu/Si interface. Examples are shown in Figure 1. η'' - Cu_3Si was found to form in samples annealed at 473 K (200 °C) for 1 hour. Plan-view and cross-sectional transmission electron microscopy (TEM) revealed that both aligned and twinned epitaxies were present. Interfacial dislocations at the silicide/Si interface were identified as edge type, with $1/2[11\bar{0}11\bar{0}]$ Burgers' vectors. The average spacing of the dislocations was measured to be 1.4 nm, which correlates well with a 15 pct mismatch at the silicide/Si interface.[4,5]

[Open image in new window](#)

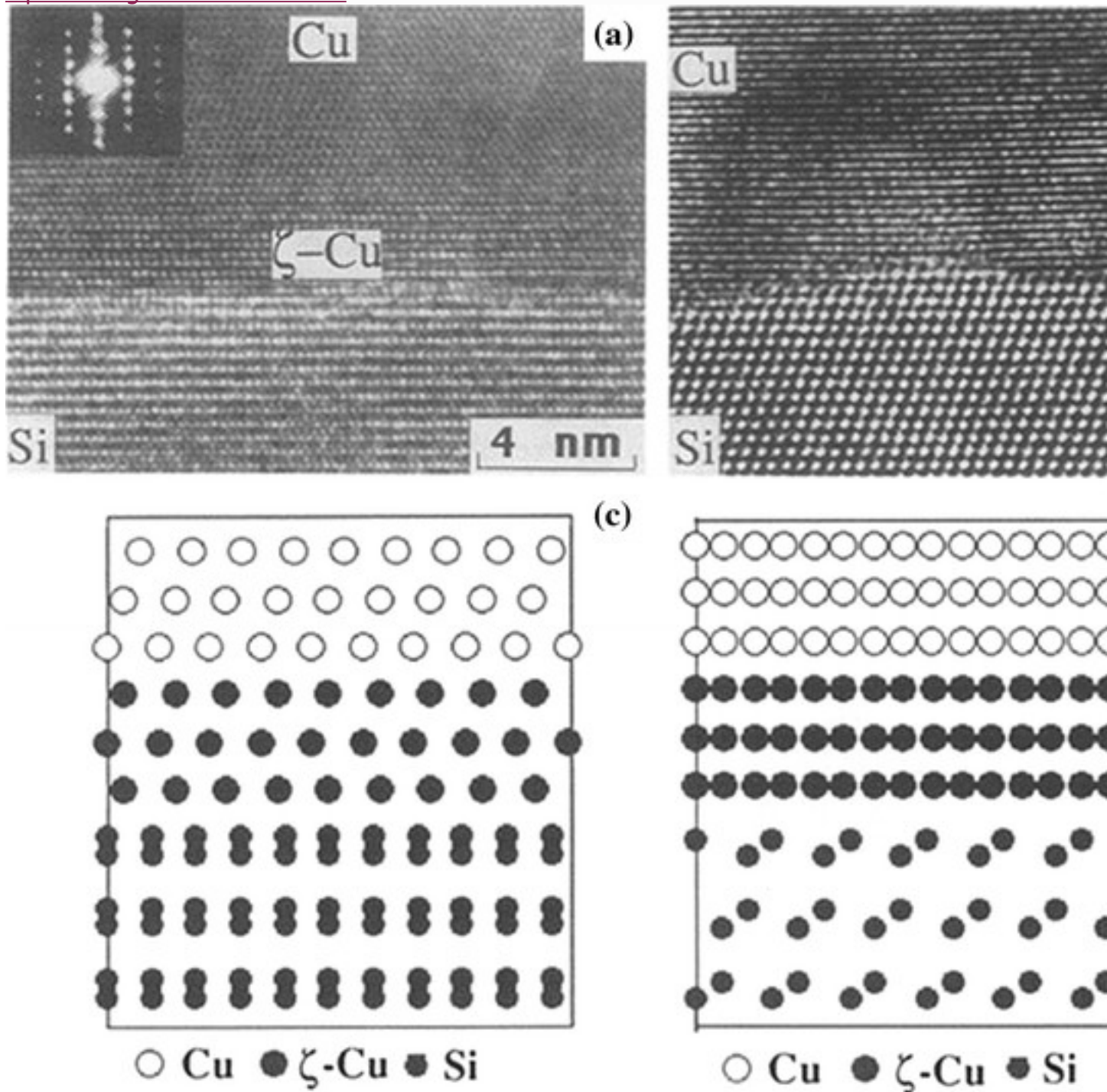


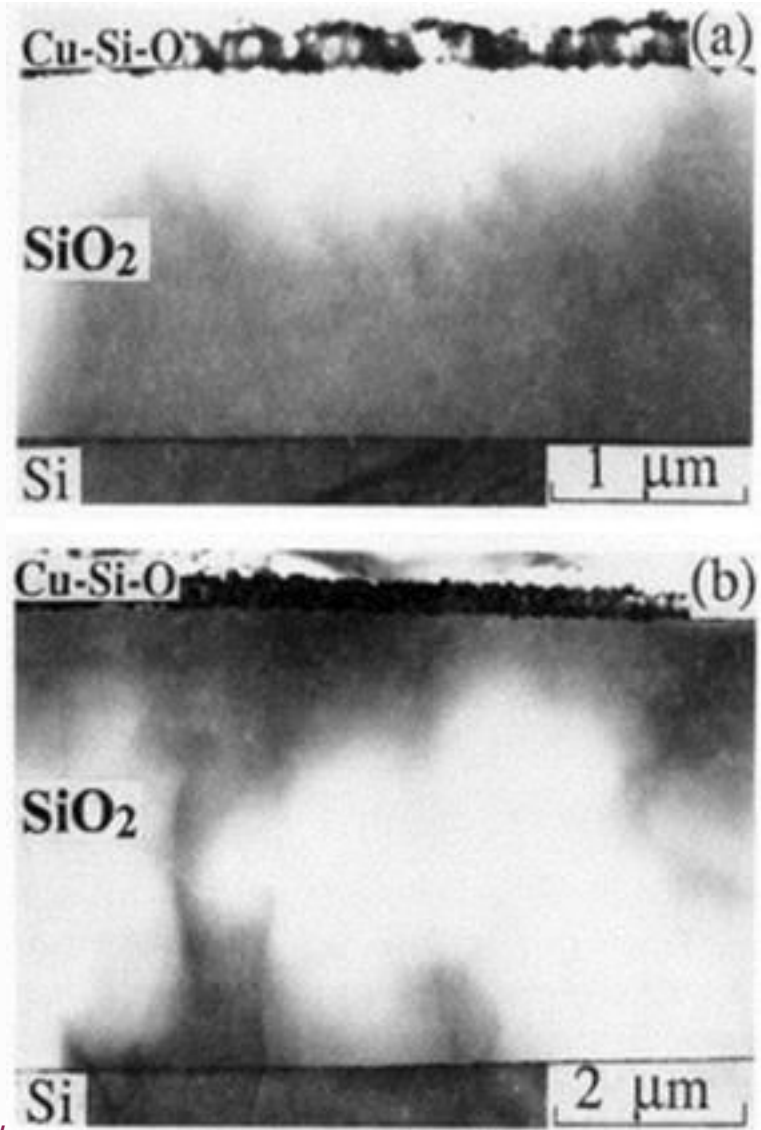
Fig. 1

Atomic images of Cu/Si interfaces along (a) $[11\bar{2}\bar{1}1\bar{2}\bar{2}]_{\text{Si}}$ and (b) $[11\bar{1}^011\bar{1}^0]_{\text{Si}}$ directions. (c) and (d) are the schematic diagrams of atomic structures corresponding to (a) and (b), respectively

Solid-phase-epitaxial growth of silicon on (111)Si through a transport media (Cu or Cu₃Si) was observed to occur at a temperature as low as 473 K (200 °C). Preferentially oriented η'' -Cu₃Si is the only phase present in samples annealed at 473 K to 1073 K (200 °C to 800 °C). In samples annealed at or higher than 1123 K (850 °C), a mixture of η' -Cu₃Si and η'' -Cu₃Si was found to be present.[5]

2.2 Room-Temperature Oxidation of Silicon Catalyzed by η'' -Cu₃Si

Room-temperature oxidation of (111)Si and (001) catalyzed by η'' -Cu₃Si has been studied. XRD analysis showed that volume fractions of η'' -Cu₃Si and Cu decrease and increase with exposure time in air ambient, respectively. From TEM diffraction analysis, Cu precipitates were found to be epitaxially related to Si. After prolonged exposure in air, the Cu precipitates were found to form an irregular network structure in the SiO₂ layer. Examination of the same area of annealed samples with intermittent exposure in air indicated that the oxidation was mainly initiated at the grain boundaries. Significant differences in room-temperature oxidation behavior between (111) and (001) samples were found.[6] The extent of oxidation was found to depend critically on the starting film thickness of Cu₃Si. The oxidation was found to be more restricted on (111)Si than that in (001)Si samples. The SiO₂ layer thickness was found to decrease with the average grain size of the starting Cu₃Si layer. High-resolution TEM revealed that the oxidation is initiated at the grain boundaries. An oxide film as thick as 4.5 μ m was grown at room temperature over a period of 2 weeks in (001) samples. The growth of the thick oxide film was achieved by minimizing the grain size of Cu₃Si through a reaction between Cu and an intermediate amorphous silicon layer at 473 K (200 °C). Examples are shown in Figure 2.[7,8] Mechanisms for catalytic oxidation of silicon in the presence of Cu₃Si are discussed. For η'' -Cu₃Si thin layer on (001)Si, the thickness of starting Cu, hence Cu₃Si, layer on silicon was found to be a critical factor in determining the oxidation behavior. Based on the microstructural evolution data, a partial reconstitution of catalytic Cu₃Si mechanism is proposed to be the dominant process for the room-temperature oxidation of silicon catalyzed by Cu₃Si.[9]



[Open image in new window](#)

Fig. 2

Cross-section TEM, bright-field images of Cu (100 nm)/a-Si (30 nm)/(001)Si samples annealed at 473 K (200 °C) for 1 h and exposed in air for (a) 1 and (b) 2 weeks

The growth kinetics of the oxidation of Si catalyzed by 170-nm-thick Cu_3Si at elevated temperatures has been investigated. For wet oxidation at 413 K to 453 K (140 °C to 180 °C), the thickness of the oxide was found to increase parabolically with time with activation energy of 0.4 ± 0.2 eV. The activation energy is close to that of diffusivity of Cu in Si. At 453 K to 473 K (180 °C to 200 °C), the growth rate became slower with increasing temperature. The growth of oxide tended to be discontinuous at the surface as the oxidation temperature was increased to a temperature at or higher than 573 K (300 °C). The anomalously fast growth of oxide at low temperatures is attributed to the presence of filamentary structures of Cu clusters in the

oxide to expedite the diffusion of the oxidants through oxide. At 473 K to 523 K (200 °C to 250 °C), more Cu atoms diffuse to the Cu₃Si/Si interface and less Cu atoms stay in the oxide, which slows down the oxide growth. The lack of filamentary structures of Cu as diffusion paths retards the growth of SiO₂. At 573 K (300 °C) or higher temperatures, the lack of filamentary structures of Cu clusters stopped the growth of continuous oxide layer altogether.[10]

2.3 Electromigration-Induced Atomic Diffusion in the Twin-Modified Cu Grain Boundaries

Grain boundaries affect the migration of atoms and electrons in polycrystalline solids, thus influencing many of the mechanical and electrical properties. By introducing nanometer-scale twin defects into copper grains, grain-boundary structure and atomic diffusion behavior are changed along the boundary. Using *in situ* ultrahigh-vacuum and high-resolution TEM, electromigration-induced atomic diffusion in the twin-modified grain boundaries was observed. The triple point where a twin boundary meets a grain boundary was found to slow down grain-boundary and surface electromigration by one order of magnitude. Examples are shown in Figure 3. It is proposed that this occurs because of the incubation time of nucleation of a new step at the triple points. The long incubation time slows down the overall rate of atomic transport.[11,12]

[Open image in new window](#)

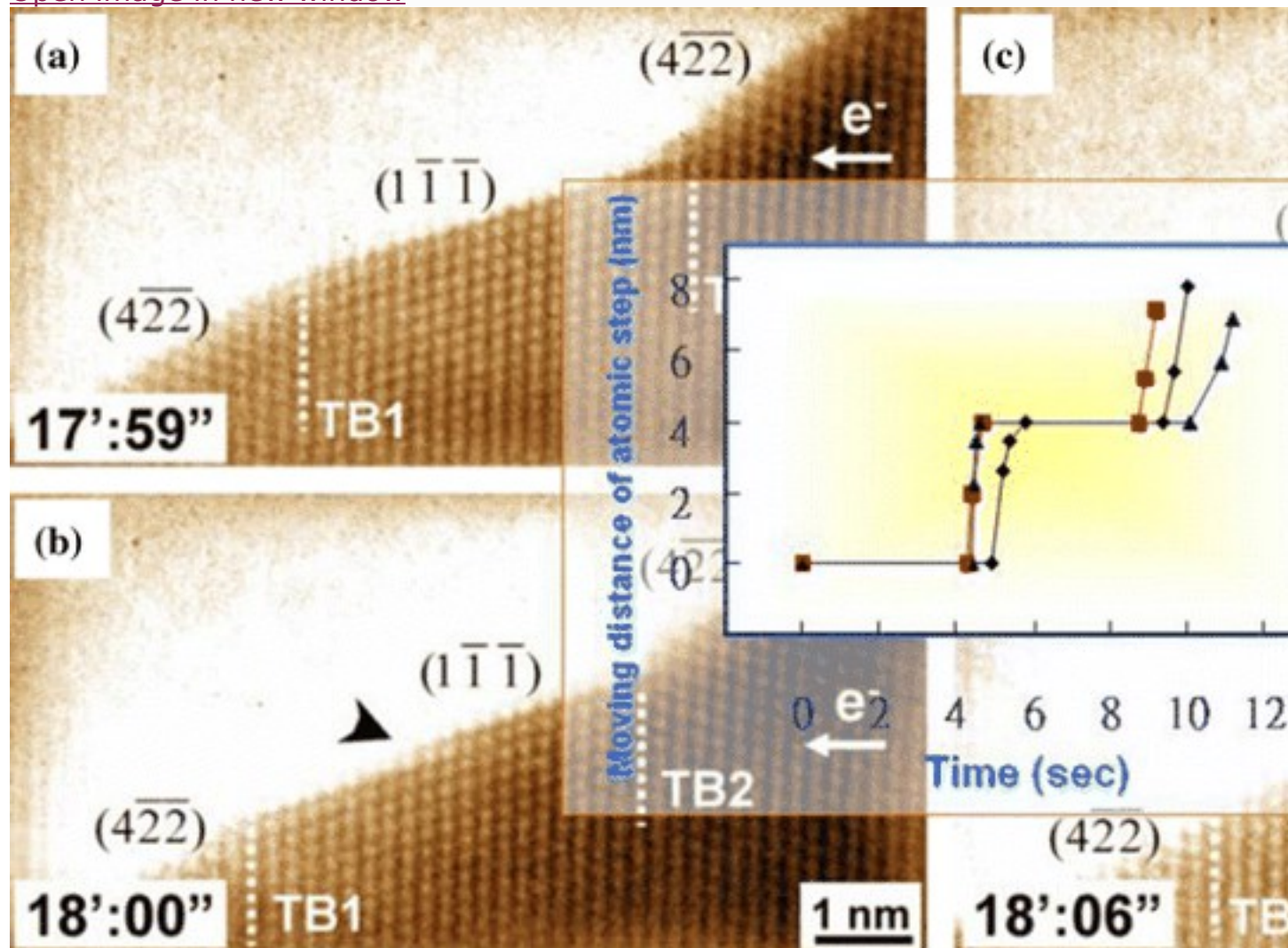


Fig. 3

(a to d) HRTEM images of the [011]-oriented Cu grain under electric current stressing as a function of time. The time of the image capture (in minutes and seconds) is given in the rectangular box at the lower left corner. The direction of electron flow is from right to left. The arrowheads indicate the atomic steps on the lattice planes. The cross in each panel refers to a fixed point for ease of inspection. Inset shows the moving distance of atomic step as a function of time

3 Advanced Device Applications

In recent years, a number of Cu and Cu alloy nanostructures were grown. [13,14] The section will mainly cover the nanoscale Cu and Cu alloys with functionalities.

3.1 Cu Nanobats as Field Emitters

The metal-organic chemical vapor deposition (MOCVD) method has been used to grow Cu nanorods without metal catalysts. Pentagonal bat-shaped Cu nanorods (Cu nanobats) with fivefold symmetry were successfully synthesized by MOCVD without capping reagents. The average diameters of the head and tail of the Cu nanobats are 100 and 50 nm, respectively. The Cu nanobats are evolved from multiple-twinned particles with a decahedral shape. Both elongation along the fivefold symmetry axis and lateral growth of exterior twins were found to be important in the growth of pentagonal Cu nanobats. An example is shown in Figure 4. The Cu nanobats possess strong field emission characteristics.[15]

[Open image in new window](#)

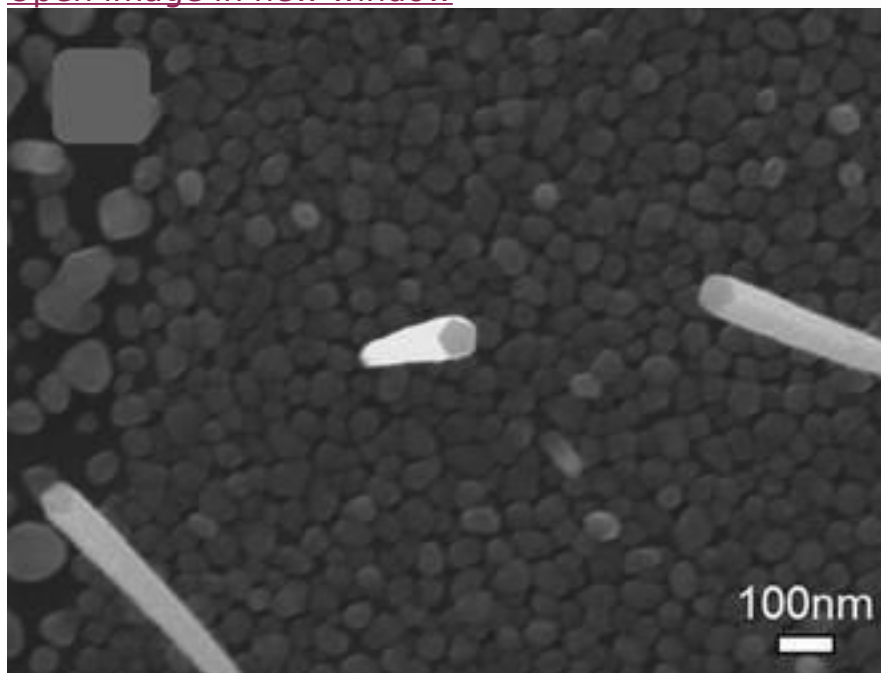


Fig. 4

Oblique-view FESEM image of pentagonal Cu nanobats grown on TaN substrate

3.2 Copper Sulfide Nanowire Array as High-Rate Capability and High-Capacity Cathodes for Lithium-Ion Batteries

A general solution method for the growth of highly ordered large-scale Cu_2S nanowire arrays onto the copper metal current collector substrates has been developed. The electrochemical behaviors of Cu_2S nanowire array cathodes for lithium-ion battery applications reveal that they exhibit stable lithium-ion insertion/extraction reversibility, high reversible lithium storage capacity, long cycle life, and outstanding rate capability. Figure 5 shows cycle performance of the Cu_2S nanowire array/Li cell circulated at a high rate of 2C. The superb electrochemical performance can be attributed to the nanowire arrays having increased reaction sites, improved cycle life in the face of mechanical strain, and efficient charge transport. With the simplicity of fabrication and good electrochemical properties, the Cu_2S nanowire arrays

are promising cathode materials for the practical use in the next generation lithium-ion batteries.[16,17]

[Open image in new window](#)

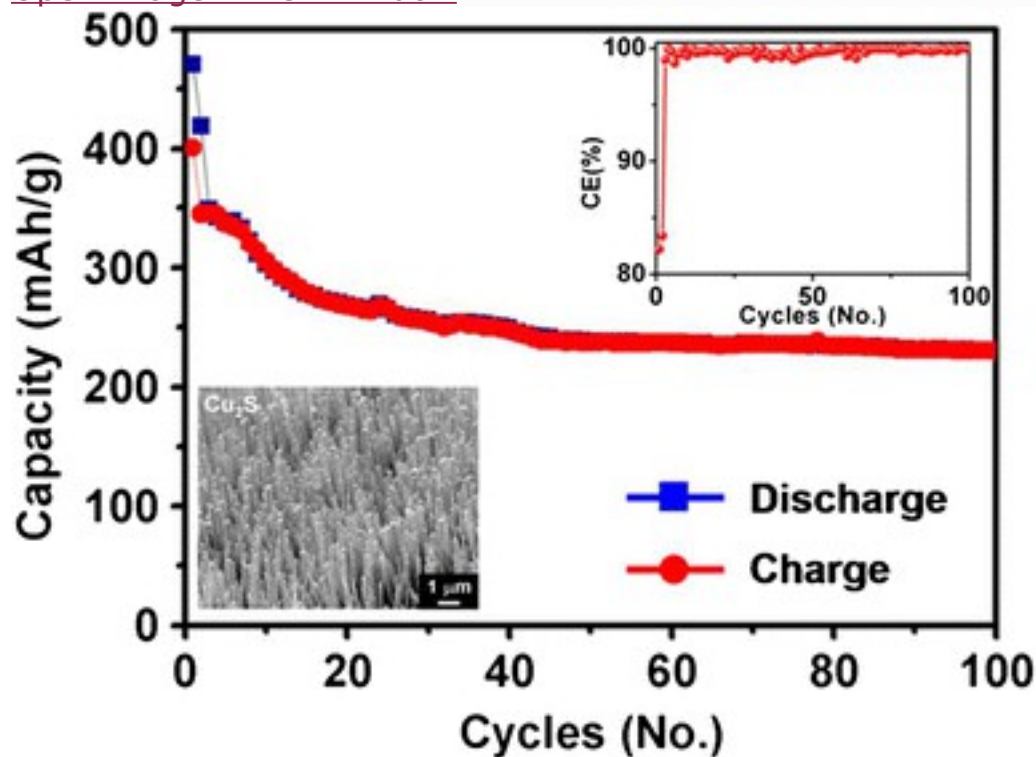


Fig. 5

Cycle performance of the Cu_2S nanowire array/Li cell circulated at a high rate of 2C. The square symbols represent the discharge cycle and the circular symbols represent the charge cycle. The inset shows the corresponding Coulombic efficiency (CE) of the Cu_2S nanowire array/Li cell

3.3 Copper Telluride Nanostructures for Field-Effect Transistors

By precisely controlling different ethylenediamine (EDA) ratios in a reaction solution, the phases and morphologies of Cu-Te nanostructures were controlled from Te/Cu core-shell nanowires at a low volume fraction of EDA <8 pct, Cu_3Te_2 nanowires at the volume fraction of EDA between 8 and 24 pct, Cu_2Te nanowires and nanobelts at the volume fraction of EDA between 24 and 48 pct, to $\text{Cu}_2\text{Te}/\text{Cu}$ core-shell nanobelts at the volume fraction of EDA over 48 pct. The formation mechanism is attributed to varied tendency of different coordinative copper complexes. *In situ* heating XRD results and TEM observations of the Cu_2Te nanowires reveal the phase transition from hexagonal $P3m1$, hexagonal $P6/mmm$ to cubic structure at annealing temperatures of 298 K, 773 K, to 873 K (25 °C, 500 °C, to 600 °C), respectively. The lack of back gate dependence demonstrates the metallic feature of Te/Cu core-shell nanowire while obvious p-type behavior can be found for Cu_2Te nanowire with an on/off ratio of $\sim 10^4$ and the field-effect hole mobility of $\sim 18 \text{ cm}^2 \text{ V}^{-1} \text{ s}^{-1}$. These Cu-Te nanostructures exhibit controllable

transport behaviors from metallic to semiconducting natures with different EDA volume fractions and have promising applications in electronics such as nonvolatile memory, photodetectors, and solar cells.[18]

3.4 Cu₃Si Nanowires as High-Performance Field Emitters and Efficient Anti-reflective Layers

Single-crystalline Cu₃Si nanowire arrays were synthesized in an organic solvent. Self-catalyzed, dense single-crystalline Cu₃Si nanowire arrays were synthesized by thermal decomposition of mono phenylsilane in the presence of copper films or copper substrates at 693 K to 748 K (420 °C to 475 °C) and 10.3 MPa in supercritical benzene. The solution-grown Cu₃Si nanowire arrays serve dual functions as field emitters and anti-reflective layers, which were reported on copper silicide materials for the first time. Cu₃Si nanowires exhibit superior field emission properties, with a turn-on-voltage as low as 1.16 V μm^{-1} , an emission current density of 8 mA cm^{-2} at 4.9 V μm^{-1} , and a field enhancement factor (β) of 1500. Cu₃Si nanowire arrays appear black with optical reflectance less than 5 pct between 400 and 800 nm serving as highly efficient anti-reflective layers. Moreover, the Cu₃Si nanowires could be grown on either rigid or flexible substrates (PI). This study showed that solution-phase silicide reactions are adaptable for high-quality silicide nanowire growth and demonstrated their promise toward fabrication of metal silicide-based devices.[19,20]

3.5 Single-Crystal Cu(In,Ga)Se₂ Nanotip Arrays for High-Efficiency Solar Cell

Direct formation of large area Cu(In,Ga)Se₂ nanotip arrays (GIGS NTRs) has been realized by using one step Ar⁺ milling process without template. By controlling milling time and incident angles, the length of CIGS NTRs with adjustable tilting orientations can be precisely controlled. Formation criteria of these CIGS NTRs have been discussed in terms of surface curvature, multiple components, and crystal quality, resulting in a highly anisotropic milling effect. The CIGS NTRs have very low reflectance <0.1 pct at incident wavelengths between 300 and 1200 nm. Open circuit voltage and short circuit current of CIGS NTRs solar cell were measured to ~390 mV and ~22.56 mA/cm², yielding the filling factor and the efficiency of 59 and 5.2 pct, respectively. In contrast to CIGS thin-film solar cell with efficiency of 3.2 pct, the nanostructured CIGS NTRs can have efficiency enhancement of ~160 pct due to the higher light absorption ability because of the nanostructure. The merits of current approach include the latest way *via* template-free direct creating process of nanostructured CIGS NTRs with controllable dimensionality and large-scale production without postselenization process.[21]

3.6 Multilevel Cu₂S Resistive Memory

Owing to the enormous demand for data storage and its self-powering potential, resistive random access memory (ReRAM) devices have received much attention. Multilevel memory is advantageous in terms of efficiency and energy saving. Multilevel resistance has been demonstrated for devices based on individual Cu₂S nanowires with two inert (W) electrodes. Up to five levels can be achieved, significantly enhancing the data storage density, by varying the compliance current (C.C.). Compared to previous works on multilevel memory, the present devices exhibit outstanding performances with lower operating voltage ($V_{\text{set}} < 0.6$ V at $I_{\text{c.c.}} = 1$ μ A), higher on/off ratio ($>10^5$), and longer retention time ($>10^3$ minutes). The typical I - V curves of single nanowire without Cu as electrode in *in situ* SEM probe system are shown in Figure 6. The SEM image of the W tips and nanowires are shown in the inset figure. From *in situ* scanning electron microscopy (SEM) and TEM analysis, the resistive switching (RS) behavior of Cu₂S nanowires under high C.C. (>1 μ A) was found to be dominated by Cu ion diffusion inside the Cu₂S nanowire. On the other hand, holes and vacant Cu lattice sites control the RS under low C.C. (<800 nA). The results of temperature-dependent measurements of resistivity also strongly support the proposed mechanisms. The facile fabrication of Cu₂S nanowires with the capability of multilevel switching shall facilitate the realization of high-density memristor applications.[22]

[Open image in new window](#)

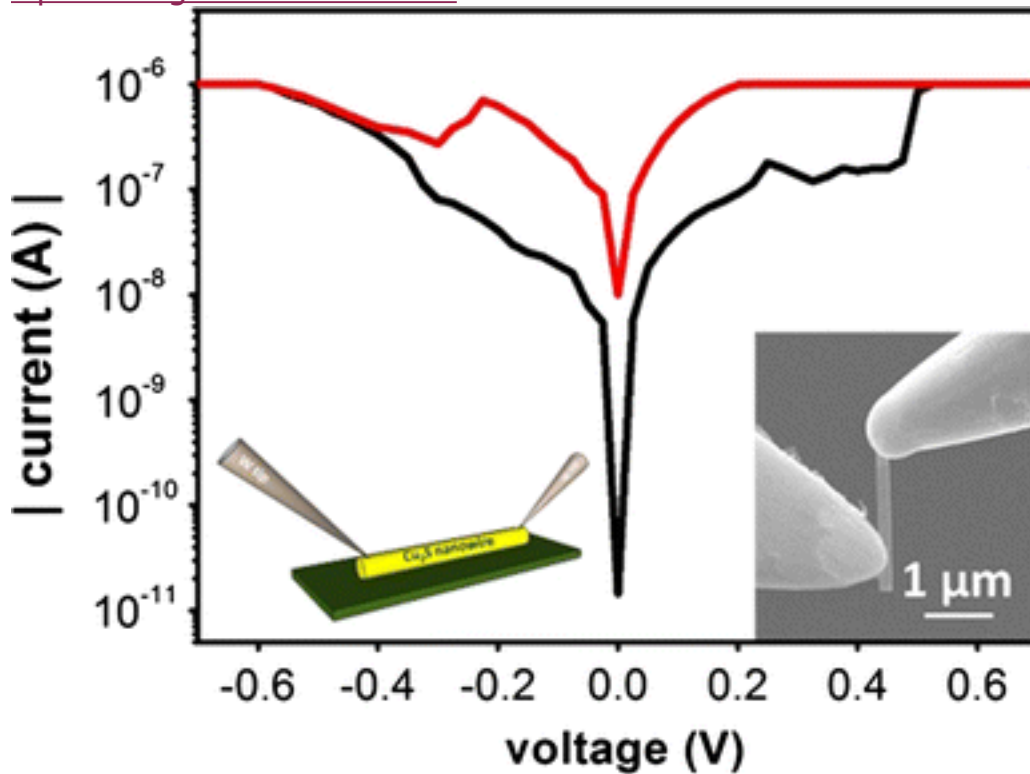


Fig. 6

Typical I - V curves of single nanowire without Cu as electrode in *in situ* SEM probe system. The SEM image of the W tips and nanowires are shown in the inset figure

3.7 Superlattice Cu_2S - Ag_2S Heterojunction Diodes

Fabrication of superlattice nanowires (NWs) with precisely controlled segments normally requires sequential introduction of reagents to the growing wires at elevated temperatures and low pressure. Here, we demonstrate the fabrication of superlattice NWs possessing multiple p - n heterojunctions by converting the initially formed CdS to Cu_2S NWs first and then to segmented Cu_2S - Ag_2S NWs through sequential cation exchange at low temperatures. In the formation of Cu_2S NWs, twin boundaries generated along the NWs act as the preferred sites to initiate the nucleation and growth of Ag_2S segments. Varying the immersion time of Cu_2S NWs in a AgNO_3 solution controls the Ag_2S segment length. Adjacent Cu_2S and Ag_2S segments in a NW were found to display the typical electrical behavior of a p - n junction. Examples are shown in Figure 7.[23,24]

[Open image in new window](#)

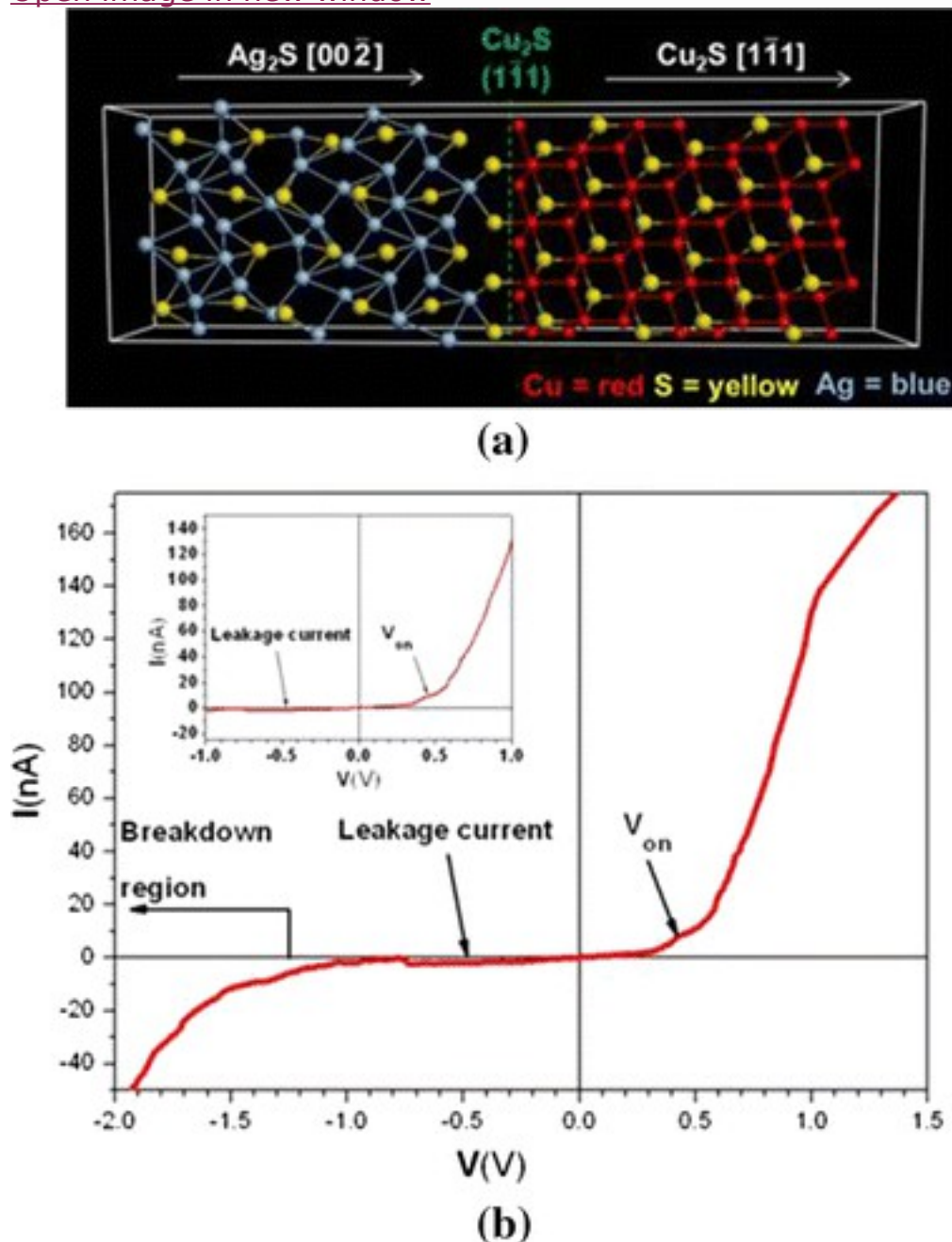


Fig. 7

(a) Crystal structure model of a $\text{Ag}_2\text{S-Cu}_2\text{S}$ p - n heterojunction. The crystal lattice directions are indicated. (b) I - V curve of the p - n heterojunction. (c) SEM images of a single superlattice NW before (upper image) and during (lower image) the contact of tungsten probes. The red circle (or darker region) and the yellow circle (brighter region) refer to the Cu_2S and Ag_2S segments, respectively. The light dot indicates a dirt near the NW as a marker to ensure the probing of the correct p - n position (Color figure online)

3.8 Facet-Dependent Cu_2O Diode

It is interesting to examine facet-dependent electrical properties of single Cu_2O crystals, since such study greatly advances our understanding of various facet effects exhibited by semiconductors. Here, we show a Cu_2O octahedron is highly conductive, a cube is moderately conductive, and a rhombic dodecahedron is nonconductive. The conductivity differences are ascribed to the presence of a thin surface layer having different degrees of band bending. When electrical connection was made on two different facets of a rhombicuboctahedron, a diode-like response was obtained, demonstrating the potential of using single polyhedral nanocrystals as functional electronic components. Density of state (DOS) plots for three layers of Cu_2O (111), (100), and (110) planes show respective metallic, semimetal, and semiconducting band structures. By examining DOS plots for varying number of planes, the surface layer thicknesses responsible for the facet-dependent electrical properties of Cu_2O crystals have been determined to be below 1.5 nm for these facets.[25]

4 Summary and Conclusions

Copper and copper alloys are a unique class of materials. They are richly endowed with favorable physical and chemical properties. Its relative ease in extraction as well as abundance in the earth crust made it the earliest metal to be used for large quantity. From ancient, medieval to modern times, they are widely used because their excellent electrical and thermal conductivities, outstanding resistance to corrosion, and ease of fabrication, together with good strength and fatigue resistance. It is rather remarkable that in the Twenty-first century, Cu continues to find new ways into many main branches of technology. For example, Cu metallization in nanoelectronics devices, Cu oxide-based superconductors, CIGS solar materials, etc. Furthermore, discovery of intriguing properties and new applications in contemporary technology for copper and its compounds have continued. In this paper, we present several examples of nanoscale Cu and Cu compounds with their functionalities, which include field emitters, field-effect transistor, lithium-ion battery cathode, anti-reflective layer, solar cell, resistive memory, p - n heterojunction diode, and facet-dependent diodes.

Judging from the tremendous progresses made in recent years, it is expected that in the nanotechnology era, a wide range of novel Cu alloy nanostructures with advanced applications will be further fruitfully explored.

Notes

Acknowledgment

The author acknowledges the support of the Ministry of Science and Technology of Taiwan under Project Numbers MOST 104-2221-E-007-030-MY3 and MOST 102-2633-M-007-002.

References

1. 1.
Copper Development Council, <http://copperalliance.org.uk/>, 2015.
2. 2.
V. Johnson, Introduction to Engineering Materials, 3rd Edition. MacMillan Press Ltd, London, 1993, pp. 202-211. [Google Scholar](#)
3. 3.
ASM Handbook, Volume 2 - Properties and Selection: Nonferrous Alloys and Special-Purpose Materials, 9th Edition, American Society for Metals, Metals Park, Ohio, USA, 1979, pp. 239-247. [Google Scholar](#)
4. 4.
C.S. Liu and L.J. Chen, J. Appl. Phys. 1993, vol. 74, pp5501-5506. [CrossRefGoogle Scholar](#)
5. 5.
C.S. Liu, S.R. Chen, W.J. Chen, and L.J. Chen, Mater. Chem. Phys. 1993, vol. 36, pp. 170-173. [CrossRefGoogle Scholar](#)
6. 6.
C.S. Liu and L.J. Chen, J. Appl. Phys. 1993, vol. 74, pp. 5507-5509. [CrossRefGoogle Scholar](#)
7. 7.
C.S. Liu and L.J. Chen, J. Appl. Phys. 1993, vol. 74, pp. 3611-3613 . [CrossRefGoogle Scholar](#)
8. 8.
C.S. Liu and L.J. Chen, J. Appl. Phys. 1994, vol. 75, pp. 2730-2732. [CrossRefGoogle Scholar](#)
9. 9.
C.S. Liu and L.J. Chen, Thin Solid Films 1995, vol. 262, pp. 187-198. [CrossRefGoogle Scholar](#)

10. 10.

H.Y. Huang and L.J. Chen, J. Appl. Phys. 2000, vol. 88, pp. 1412-1417.[CrossRefGoogle Scholar](#)

11. 11.

K.C. Chen, W.W. Wu, C.N. Liao, L.J. Chen, and K.N. Tu, Science 2008, vol. 321, pp. 1066-1069.[CrossRefGoogle Scholar](#)

12. 12.

L.J. Chen and W.W. Wu, Mater. Sci. Engineering R, 2010, vol. 70, pp. 303-319 .[CrossRefGoogle Scholar](#)

13. 13.

Y. Chang, M.L. Lye and H.C. Zeng, Langmuir, 2005, vol. 21, pp. 3746-3748.[CrossRefGoogle Scholar](#)

14. 14.

J. H. Wang, P. Y. Su, M. Y. Lu, L. J. Chen, C. H. Chen, and C. J. Chiu, Solid-State Lett. 2005, vol. 8, pp. C9-C11.[CrossRefGoogle Scholar](#)

15. 15.

J. H. Wang, T. H. Yang, W. W. Wu, L. J. Chen, C.H. Chen, and C.J. Chiu, Nanotechnology, 2006, vol. 17, pp. 719-722.[CrossRefGoogle Scholar](#)

16. 16.

C.H. Lai, K.W. Huang, J.H. Cheng, C.Y. Lee, B.J. Hwang, and L.J. Chen, J. Mater. Chem. 2010, vol. 20, pp. 6638-45.[CrossRefGoogle Scholar](#)

17. 17.

C.H. Lai, M.Y. Lu, and L.J. Chen, J. Mater. Chem. 2012, vol. 22, pp. 19-30.[CrossRefGoogle Scholar](#)

18. 18.

C.C. Lin, W.F. Lee, M.Y. Lu, S.Y. Chen, M.H. Lung, T.C. Chan, H.W. Tsai, Y.L. Chueh, and L.J. Chen, J. Mater. Chem. 2012, vol. 22, pp. 7098-7103.[CrossRefGoogle Scholar](#)

19. 19.

Fang-Wei Yuan, Chiu-Yen Wang, Lih-Juann Chen, Hsing-Yu Tuan, and Kang L. Wang, *Nanoscale* 2013, vol. 5, pp. 9875- 81.[CrossRefGoogle Scholar](#)

20. 20.

L.J. Chen and W.W. Wu, *Jpn. J. Appl. Phys.* 2015, vol. 54, pp. 07JA01-1-11.[Google Scholar](#)

21. 21.

C.H. Hung, C.H. Chen, S.Y. Chen, Y.T. Yen, W.C. Shih, W.C. Kuo, J.Y. Juang, Y.K. Liao, H.C. Kuo, C.H. Lai, L.J. Chen, and Y.L. Chueh, *Nano Lett.* 2011, vol. 11, pp. 4443-4448.[CrossRefGoogle Scholar](#)

22. 22.

P.H. Liu, C.C. Lin, A. Manekkathodi, and L.J. Chen, *Nano Energy* 2015, vol. 15, pp. 362-368.[CrossRefGoogle Scholar](#)

23. 23.

Chih-Shan Tan, Ching-Hung Hsiao, Shau-Chieh Wang, Pei-Hsuan Liu, Ming-Yen Lu, Michael H. Huang, Hao Ouyang, and Lih-Juann Chen, *ACS Nano* 2014, vol. 8, pp. 9422-9426.[CrossRefGoogle Scholar](#)

24. 24.

Chih-Shan Tan, Hung-Ying Chen, Hsueh-Szu Chen, Shangjr Gwo, Lih-Juann Chen, *Scientific Reports*, 2015, vol. 5, pp. 13759-1-7.[Google Scholar](#)

25. 25.

Chih-Shan Tan, Shih-Chen Hsu, Wei-Hong Ke, Lih-Juann Chen, and Michael Huang, *Nano Lett.* 2015, vol. 15, pp. 2155-2160.[CrossRefGoogle Scholar](#)